Received: 21 August 2019 | Revised: 19 March 2020 | Accepted: 7 May 2020

DOI: 10.1002/we.2527

WILEY

RESEARCH ARTICLE

Improving wind speed forecasts from the Weather Research and Forecasting model at a wind farm in the semiarid Coquimbo region in central Chile

Ignacio Salfate[1] | Julio C. Marin[2,4] | Omar Cuevas[3,4] | Sonia Montecinos[1]

[1]Departamento de Física y Astronomía, Universidad de La Serena, La Serena, Chile

[2]Departamento de Meteorología, Universidad de Valparaíso, Valparaíso, Chile

[3]Instituto de Física y Astronomía, Universidad de Valparaíso, Valparaíso, Chile

[4]Centro Interdisciplinario de Estudios Atmosféricos y Astroestadística, Universidad de Valparaíso, Valparaíso, Chile

Correspondence
Julio C. Marin, Departamento de Meteorología, Universidad de Valparaíso, Gran Bretaña #644, Playa Ancha, Valparaíso, Chile.
Email: julio.marin@uv.cl

Funding information
Fondo de Fomento al Desarrollo Científico y Tecnológico; FONDEF IDeA, Grant/Award Number: ID14I10016; Dirección de Investigación y Desarrollo de la Universidad de La Serena University (DIDULS), Grant/Award Number: PI15141; Departamento de Física y Astronomía of Universidad de La Serena; Centro de Estudios Atmosféricos y Astroestadística (CEAAS) of Universidad de Valparaíso

Peer Review
The peer review history for this article is available at https://publons.com/publon/10.1002/we.2527.

Abstract

Accurate predictions of the wind field are key for better wind power forecasts. Wind speed forecasts from numerical weather models present differences with observations, especially in places with complex topography, such as the north of Chile. The present study has two goals: (a) to find the WRF model boundary layer (PBL) scheme that best reproduces the observations at the Totoral Wind Farm, located in the semiarid Coquimbo region in north-central Chile, and (b) to use an artificial neural network (ANN) to postprocess wind speed forecasts from different model domains to analyze the sensitivity to horizontal resolution. The WRF model was run with three different PBL schemes (MYNN, MYNN3, and QNSE) for 2013. The WRF simulation with the QNSE scheme showed the best agreement with observations at the wind farm, and its outputs were postprocessed using two ANNs with two algorithms: backpropagation (BP) and particle swarm optimization (PSO). These two ANNs were applied to the innermost WRF domains with 3-km (d03) and 1-km (d04) horizontal resolutions. The root-mean-square errors (RMSEs) between raw WRF forecasts and observations for d03 and d04 were 2.7 and 2.4 ms^{-1}, respectively. When both ANN models (BP and PSO) were applied to Domains d03 and d04, the RMSE decreased to values lower than 1.7 ms^{-1}, and they showed similar performances, supporting the use of an ANN to postprocess a three-nested WRF domain configuration to provide more accurate forecasts in advance for the region.

KEYWORDS
ANN postprocessing, numerical weather prediction model forecasts, PBL parameterizations, wind power

1 | INTRODUCTION

The wind power generation has experienced rapid development in the last decades due to its low cost and large technological advancements compared with other renewable energy sources.[1,2]

Abbreviations: ANN, artificial neural network; AWS, atmospheric weather station; BP, backpropagation; CEAZA, Centro de Estudios Avanzados en Zonas Aridas; ENSO, El Niño Southern Oscillation; FNL, final analysis; MFNN, multilayer feed-forward neural network; MJO, Madden–Julian oscillation; MYNN, Mellor–Yamada Nakanishi and Niino; NCEP, National Centers for Environmental Prediction; NWP, numerical weather prediction; PBL, planetary boundary layer; PSO, particle swarm optimization; QNSE, Quasi-Normal Scale Elimination; *R*, correlation coefficient; RMSE, root-mean-square error; SS, skill score; WRF, Weather Research and Forecasting.

The Coquimbo region is located in the semiarid northern part of Chile between 29° S and 32° S (Figure 1). It is known as a transitional zone between the hyperarid Atacama Desert to the north and the mesic Mediterranean climate of central Chile.[3] The region is bounded by the Andes Cordillera to the east and the Pacific Ocean to the west. Large-scale factors, such as the Southeast Pacific subtropical anticyclone and cold lows from the west, influence the region on a seasonal basis.[4,5] The Southeast Pacific anticyclone displaces from south of 35° S in summer to north of 27° S in winter, allowing the passage of extra-tropical cyclonic perturbations over the region, which results in a larger wind speed seasonal variability during winter. In addition, the largest wind speeds occur in the spring months. On the other hand, large interannual (from 1 year to the next) and intraseasonal (within a season) variations in precipitation and atmospheric circulations have been associated with El Niño Southern Oscillation (ENSO)[4,6,7] and Madden-Julian Oscillations (MJO),[8,9] respectively. The alongshore wind in the region decreases during the warm ENSO phase (El Niño) and increases during the cold phase (La Niña), associated with variations in the north-south pressure gradient,[4,10] whereas cyclonic/anticyclonic circulations and low/high-pressure anomalies are related to different phases of the MJO, causing wind speed variations at subseasonal scales.[9] At diurnal timescales, sea and valley breezes have varying importance, depending on location in the complex topography and time of the year.[11]

Chile is moving toward a policy of decarbonization of the energy matrix. Currently, 21% of the energy matrix corresponds to nonconventional renewable energies, 7% of which corresponds to wind energy, and 10% to solar energy. The Coquimbo region concentrates 67% of the installed wind power capacity of the country (about 700 MW). Because the wind has become an important clean energy source for the region, its accurate prediction will provide reliable wind energy forecasts, favoring the region's economic and social development.

Due to the largely variable nature of wind speed, having a method to accurately estimate it, has become a major technological challenge. There are different techniques to model the wind behavior, which can be classified as (i) physical models, (ii) conventional statistical models, (iii) spatial correlation models, and (iv) artificial intelligence. A review of these methods can be found in Costa et al., [12] Lei et al., [13] Aggarwal and Gupta,[14] and Chang.[15] One of the most used physical methods is the numerical weather prediction (NWP) model, which can provide wind forecasts in a region at spatial resolutions that range from few hundred kilometers to few meters.[16,17] However, it is well known that forecasts from NWP models can show systematic errors, especially in places of complex topography,[18-20] as it is found in the Coquimbo region and along continental Chile.

The accuracy of wind speed forecasts in the planetary boundary layer (PBL) is affected by the ability of the model to represent PBL processes. This drawback is attributed in part to the misrepresentation of the real topography in the model, and difficulties of PBL and atmospheric stability assumptions related to how the near surface wind is represented. The Weather Research and Forecasting (WRF) model offers several schemes of different characteristics and complexity to model the PBL processes. Many authors have evaluated the performance of different PBL schemes in the WRF model to choose the one that shows the best agreement with observations in regions of interest for wind energy production.[21-24] However, it is important to note that the best configuration chosen for one region and period of the year may not show the same performance for another region. For that reason, a sensitivity analysis of the model parameterizations should be first conducted for each region of study.

Several studies have been conducted in recent years to investigate different aspects of wind power generation in Chile. Watts and Jara[25] analyzed several wind profile observations in northern Chile to discuss the suitability of wind power generation. A method to estimate wind potential from observations and a diagnostic model were proposed by Morales et al.[26] in south-central Chile (34° −36° S). The impact of ENSO on wind power production in the Coquimbo region was studied by Watts et al.,[27] whereas the capacity to generate off-shore wind power potential in south-central Chile was first estimated by Mattar and Borvarán[28] using the WRF model and in situ observations. Recently, two studies performed sensitivity tests to PBL schemes and other options in Chile.[29,30] Muñoz et al.[29] described a Chilean program aimed to gather observational and

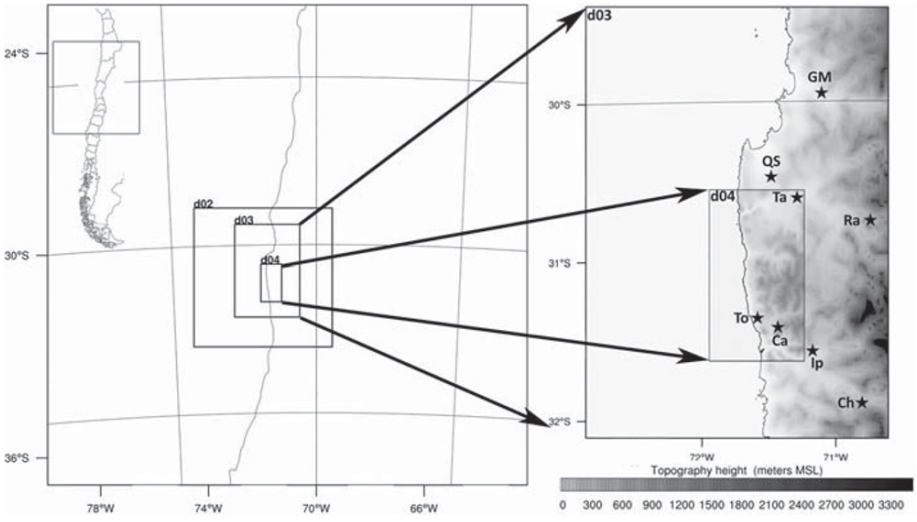

FIGURE 1 Domains used in the Weather Research and Forecasting (WRF) model centered on the Totoral Wind Farm. The zoom image shows the location of the Totoral and the atmospheric weather stations (AWSs) superposed on WRF Domains 3 and 4. The topography of the region is plotted in gray scale color

model information to support wind potential in Chile. Its study focused on the Atacama region in northern Chile, but they also conducted high-resolution (1 km) WRF numerical simulations over the whole country for 2010. On the basis of sensitivity tests over the Atacama region, they selected a set of model parameterizations that showed the best performance with observations. For the case of the PBL scheme, they selected the Quasi Normal Scale Elimination (QNSE), mainly due to its better performance to simulate nocturnal conditions such as low-level jets present in the Atacama Desert.[31] González-Alonso de Linaje et al.[30] found that the Mellor–Yamada Nakanishi and Niino Level 3 (MYNN3) PBL scheme showed the best agreement with observations in the analysis of offshore wind energy potential in the Coquimbo region using the WRF model at a horizontal resolution of 3 km for 2 months of 2013. They obtained root-mean-square error (RMSE) and determination coefficients (R^2) in the range 1.75–2.5 ms^{-1} and 0.47–0.76, respectively. Previous PBL studies evaluated the offshore wind power potential in the Coquimbo region using a 3-km horizontal resolution simulation for just 2 months[30] or evaluated the onshore wind power capacity at 1-km horizontal resolution but for another region.[29] Therefore, it would be necessary to perform a long-term (over a year) PBL sensitivity study at 1-km horizontal resolution to assess the wind speed forecast performance and its seasonal variability for onshore wind power evaluation in the Coquimbo region. Furthermore, methods to reduce systematic forecast errors should be tested.

Artificial neural networks (ANNs) have been successfully used to improve wind speed forecasts.[32-34] Wind speeds and wind energy potential up to 72 h were predicted using a recurrent neural network in Barbounis et al.[35] Their results were compared with the persistence method obtaining a 50% of improvement for forecast windows larger than 20 h. Five different data mining algorithms were used by Kusiak et al.[36] to predict wind speed and wind power, highlighting the ANN approach over the others. A feed-forward neural network in combination with wavelet transform was used by Catalão et al.[37] to forecast short-term wind power in Portugal. Their results outperformed the persistence and other methods more complex. On the other hand, the particle swarm optimization (PSO) algorithm, which was proposed by Kennedy and Eberhart,[38] has been a popular optimization algorithm due to its easy use and implementation. A number of studies have used the PSO algorithm in different problems related to wind energy, such as finding the optimal distribution of wind turbines in a farm,[39] determining wind turbine characteristics to increase the wind power efficiency,[40] and designing wind turbine blades to reduce production costs.[41] It was also employed by Liu et al.[42] to predict nonstationary wind speeds. An ANN with PSO and backpropagation (BP) algorithms was implemented in the current study in order to post-process wind speed forecasts and reduce its errors. Details will be given below.

The current study focuses on the Totoral Wind Farm, which is located near the coast, in the Norte Chico of Chile (Coquimbo region) and has a total capacity of 46 MW, corresponding to 23 wind turbines with a nominal power of 2 MW each. The study aims two goals: first, to evaluate the sensitivity of three PBL parameterizations in the WRF model during 2013 to determine the one that best represents the wind field in the region of interest. The schemes chosen were the QNSE scheme based on the results obtained by Muñoz et al.[29] and Nunalee and Basu[43]; the MYNN scheme because it is used in daily operational WRF simulations by the Chilean Weather Service (personal communication); and the MYNN3, which was chosen due to its better agreement to forecast wind speeds near the coast in the Coquimbo region[30] and because it is a more complex version of MYNN. Second, a multilayer feed-forward neural network (MFNN) trained with BP and PSO algorithms was applied to wind speed forecasts from two WRF domains of different horizontal resolutions (3 and 1 km) as postprocessing techniques, aiming to improve the wind speed forecasts and consequently to provide more reliable wind energy forecasts for the region. Louka et al.[44] applied a postprocessing method (Kalman filter) to coarse-resolution model output, obtaining a better performance with observations than its high-resolution nested domain. Our second goal aims also to determine whether a postprocessing method applied to a coarser-resolution domain shows a better performance than our high-resolution nested domain, which can save computational resources and provide wind forecasts in advance for the region.

The paper is divided into the following sections: Section 2 describes the WRF model, the configurations used in the sensitivity tests to PBL schemes, and the observations used to validate the weather forecasts. Besides, the algorithms employed to train the ANN and the approaches used to improve wind speed forecasts are explained. Section 3 shows the results. The conclusions and a discussion of results are presented in Section 4.

2 | DATA AND METHODOLOGY

2.1 | Experimental data

A meteorological tower is installed at the Totoral farm to record the wind speed at 80- and 34-m height, air temperature at 77.5 m, and pressure at 3-m height. Wind speeds and temperature from seven atmospheric weather stations (AWSs) from the National Weather Service (Dirección Meteorológica de Chile)[†] and CEAZA (Centro de Estudios Avanzados en Zonas Aridas)[‡]networks were available for this study. Figure 1 shows the location of the 80-m anemometer at Totoral and the AWSs installed in the region. Their names and geographical information are shown in Table 1.

[†]www.meteochile.cl
[‡]www.ceazamet.cl

TABLE 1 Location of Totoral Wind Farm and the atmospheric weather stations (AWSs) used in this study

	Totoral (To)	Canela (Ca)	Talhuen (Ta)	Chillepin (Ch)	G. Mistral (GM)	Illapel (Ip)	Q. Seca (QS)	Rapel (Ra)
Latitude	−30.65	−31.39	−30.59	−31.88	−29.97	−31.68	−30.49	−30.72
Longitude	−70.39	−71.41	−71.24	−70.71	−71.08	−71.19	−71.49	−70.77
m.a.s.l.	246	350	292	887	198	275	183	862

Abbreviation: m.a.s.l., meters above sea level.

TABLE 2 Description of domains used in the Weather Research and Forecasting (WRF) simulations

Domain	Resolution (km)	Grid points	Area (km^2)
1	27	60 × 60	97 200
2	9	52 × 52	24 336
3	3	73 × 103	22 557
4	1	70 × 124	8680

2.2 | Numerical weather prediction model

The WRF model is a mesoscale numerical weather prediction system that is used for both operational forecasting and atmospheric research. Several research centers, agencies, and universities have contributed to developing and implementing new physics schemes, data assimilation, and numerics into the model. Besides, detailed databases for land use, topography, and soil type are provided for high-resolution forecasts. Version 3.6.1 of the model[45] was used in this study.

The WRF model was run fully compressible, nonhydrostatic, with four nested domains (Figure 1 and Table 2) and 41 vertical levels. The final global analysis (FNL), run at the National Centers for Environmental Prediction (NCEP)[§], was used as initial and boundary conditions for the WRF simulations every 6 h. The FNL data have a horizontal resolution of $1^\circ \times 1^\circ$. The simulations started every day at 18 UTC and run for 30 h. The first 6 h of simulation at each day was not used in the comparison to avoid the initial model perturbations (e.g., spin-up errors). Therefore, the diurnal evolution analysis was performed from the forecast hour 6 to 30 in the simulations, and WRF outputs were saved every 1 h.

Three PBL schemes from the WRF model were evaluated at the Totoral Wind Farm: the MYNN[46] Levels 2.5 and 3.0 (MYNN3[47]) and the QNSE.[48] The rest of physics parameterizations that were used in the simulations were the RRTM longwave radiation,[49] the Dudhia shortwave radiation,[50] the Noah land surface model,[51] and the simple ice microphysics[52] scheme, which were used in all domains, while the Kain–Fritsch cumulus parameterization[53] was used in Domains 1 and 2.

The sensitivity tests to PBL schemes were conducted from January 1 to December 31, 2013. The evaluation was performed with observations from weather stations located within Domains 3 and 4 in WRF simulations. In the case of weather stations located outside Domain 4 in our simulations, we analyzed the performance of the model in those sites using forecasts from Domain 3. We used forecasts from Domain 4 to compare with observations at Totoral Wind Farm and Canela and Talhuen AWS (see Figure 1). Wind speeds from WRF simulations were extracted at the nearest grid point to meteorological stations and the Totoral Wind Farm. In addition, WRF simulations at Totoral Wind Farm were interpolated to the anemometer altitude (80-m height). An ANN trained with two different algorithms was later applied to wind speed forecasts from Domains 3 and 4 of the WRF configuration that showed the best results at Totoral Wind Farm. The postprocessed wind speed forecasts were evaluated with raw WRF forecasts and observations during the period February 1 to December 31, 2014.

2.3 | Backpropagation neural network and PSO algorithms

An ANN can model nonlinear processes such as wind speed evolution, based on how our human body learns. We will use an ANN as a postprocessing tool to reduce the systematic errors present in wind speed forecasts from the WRF model. Among its advantages are its flexibility and ability to produce output even with incomplete information. On the other hand, important disadvantages are its sometimes unexplained functioning, and its output may sometimes be worse than the original data aimed to correct.

The MFNN using a BP algorithm is the most popular type of ANN, which commonly has three layers of neurons: the input layer, a hidden layer, and the output layer. Besides, a backing layer is connected with the previous layer using operators called weights ω. It has been shown that a hidden layer with an appropriate number of neurons is sufficient to approximate any continuous function.[37] To select the appropriate number

[§]National Centers for Environmental Prediction and National Weather Service and NOAA and US Department of Commerce, NCEP FNL Operational Model Global Tropospheric Analyses, continuing from July 1999, Research Data Archive at the National Center for Atmospheric Research, Computational and Information Systems Laboratory, Boulder, CO, 2000, https://doi.org/10.5065/D6M043C6

of neurons in the hidden layer for our study, we evaluated the RMSE during a validation period (January 2014) and chose the number of neurons that showed the smallest RMSE.

There are two main steps in the operation of ANNs: training and prediction. In the training process, the ANN modifies the weights in response to the input information.[54] For a neural network with **M** layers, the calculation of the neuron output *j* in the *l*th layer can be expressed as in Hagan and Menhaj[55]:

$$a^l{}_j = f^l{}_j\left(\sum_{i=1}\omega^l{}_{ji}a_i^{l-1} + b^l{}_j\right), \tag{1}$$

where a_i is the neuron output *i* of the previous layer (*l*−1), $f^l{}_j$ and $b^l{}_j$ correspond to the transfer function and the gain (bias) of neuron *j* in the *l*th layer, respectively, and ω_{ij} is the weight that connects neuron *j* of the *l*th layer with neuron *i* of the previous Layer l-1.

The function *f* can be linear or nonlinear. In this study, the following hyperbolic tangent equation was used as the transfer function between the input layer and the hidden layer:

$$f(a^l{}_j) = \frac{exp(a^l{}_j) - exp(-a^l{}_j)}{exp(a^l{}_j) + exp(-a^l{}_j)}, \tag{2}$$

and a linear transfer function was used between the hidden layer and the output layer (i.e., there is no activation function).

The BP algorithm for multilayer networks is a generalization of the delta learning rule.[56] It adjusts the weights and biases that modulate the connections between neurons, to minimize the mean square error between the network outputs and the expected outputs.

The PSO refers to a method that simulates swarming behavior in nature.[57] It consists of an iterative and stochastic process that operates on a group of particles where the position of each particle depicts a possible solution within a search space representing the problem to be solved. In each iteration, both the position and speed of each swarm particle are updated, leading the swarm to the optimal solution. The following equations are used to update the particle velocities (v_i) and positions (x_i):

$$v_i^{t+1} = \omega v_i^t + c_1 r_1(\varphi_i^t - x_i^t) + c_2 r_2(\varphi_g^t - x_i^t), \tag{3}$$

$$x_i^{t+1} = x_i^t + v_i^{t+1}, \tag{4}$$

where *t* is the current step, ω is the inertia weight, c_1 and c_2 are the acceleration coefficients, and r_1 and r_2 are two random variables in the range [0,1]. The terms φ_i^t and φ_g^t are the best solution reached by the particle (local exploration) and the best solution reached by the entire swarm (global exploration), respectively.

The task of the inertia weight is to exchange between the capabilities of exploration of long and short range; therefore, to have a balance between both, an appropriate value of ω must be chosen. In this study, we calculated ω using the following expression:

$$\omega = \omega_{max} - \left(\frac{\omega_{max} - \omega_{min}}{t_{max}}\right)t, \tag{5}$$

where ω_{max} and ω_{min} are the maximum and minimum inertial weight values, respectively, and t_{max} and *t* are the maximum iteration number and the current iteration value, respectively.

We used two different ANNs to improve wind speed forecasts at the Totoral Wind Farm. They differ from each other in the training algorithm used: BP and PSO. We applied both ANNs to hourly wind speed forecasts from WRF model Domain 3 (3-km horizontal resolution) and Domain 4 (1-km horizontal resolution) to analyze the impact of horizontal resolution on the corrected forecasts. As a result, four different ANN approaches were evaluated to correct wind speed forecasts at Totoral, summarized below:

- d04bp: ANN with forecasts from Domain d04 and the BP training algorithm.
- d04pso: ANN with forecasts from Domain d04 and the PSO training algorithm.
- d03bp: ANN with forecasts from Domain d03 and the BP training algorithm.
- d03pso: ANN with forecasts from Domain d03 and the PSO training algorithm.

On each of the four approaches analyzed, the ANN was trained with 11 atmospheric variables as input: wind speed and direction at 80- and 34-m height, temperature, and relative humidity at 80 m, the pressure at 3-m height, and four fuzzy logic-type membership functions that characterize the daily cycle, whose degree of membership between them is displayed in Figure 2.

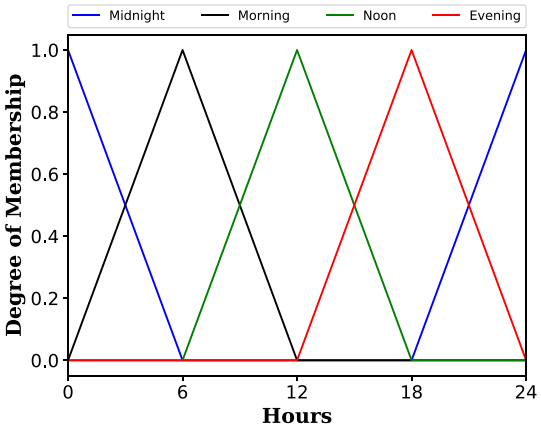

FIGURE 2 Fuzzy logic membership functions to characterize the hours of the day used as input [Colour figure can be viewed at wileyonlinelibrary.com]

The PSO algorithm was implemented with a swarm size of 25 particles. A value of 1.496 was chosen for both constants c_1 and c_2, the inertia weight ω of Equation (5) oscillates between ω_{min}=0.4 and ω_{max}=0.9, and the objective function to be minimized was the RMSE (Equation 6). The task of the PSO algorithm is to optimize the weights and the bias of the network.[58]

The whole process to select the best ANN was done by trial and error, among many tests that modified the number of input variables and changed the number of neurons in the hidden layer. The tuning PSO parameters were found in the same way. Three time periods were used in the analysis of the four ANN approaches: data from January to December 2013 were used in the training set, January 2014 was used in the validation set, where we selected the appropriate number of neurons in the hidden layer based on the RMSE value between the ANN and observations for that month, and the period February to December 2014 was used in the test set. Results from the test period, for each ANN approach, will be described in Section 3.2.

The criteria for evaluating the performance of wind speed forecasts were the bias, which quantifies the systematic error in the model, the RMSE that shows the magnitude of the error, the linear correlation coefficient (R), and the skill score (SS), which quantifies the forecast improvement based on the decrease of the RMSE.[59] These metrics were applied to wind speed forecasts from raw and ANN-corrected WRF simulations. The following equations were used to calculate the bias, RMSE, SS, and R:

$$RMSE = \sqrt{\frac{1}{N}\sum_{i=1}^{N}(x_i - y_i)^2}, \tag{6}$$

$$R = \frac{\sum_{i=1}^{N}(y_i - \bar{y})(x_i - \bar{x})}{\sqrt{\sum_{i=1}^{N}(y_i - \bar{y})^2}\sqrt{\sum_{i=1}^{N}(x_i - \bar{x})^2}}, \tag{7}$$

$$Bias = \sum_{i=1}^{N}\frac{(y_i - x_i)}{N}, \tag{8}$$

$$SS = \frac{RMSE_1 - RMSE_2}{RMSE_1} \times 100, \tag{9}$$

where y_i represents the simulated wind speed and x_i the observed value. The $RMSE_1$ and $RMSE_2$ represent the RMSE from raw and ANN-corrected WRF forecasts, respectively.

3 | RESULTS

This section is divided into two parts. In Section 3.1, we present the results of the sensitivity tests to different PBL schemes in the WRF model for the region of interest during 2013. The results of applying the four ANN approaches (d03bp, d03pso, d04bp, and d04pso) to improve wind speed forecasts at 80-m height at Totoral Wind Farm are shown in Section 3.2. Raw WRF and ANN-corrected WRF forecasts will be evaluated with observations for the period February to December 2014.

3.1 | Sensitivity analysis to PBL schemes

Wind speed and temperature forecasts from the three WRF simulations with different PBL schemes were compared with observations from five weather stations (Chillepin, Rapel, Illapel, Q. Seca, and G. Mistral) located in Domain 3 (3-km horizontal resolution) and with two weather stations (Canela, Talhuen) and the 80-m anemometer at Totoral located in Domain 4 (Figure 1) to analyze the performance of the model in the region. Because the size of Domain 4 is not large enough (due to computer power and storage limitations) to encompass all the stations of the region, we used results from Domain 3 to complement the comparison with observations. Table 3 shows that MYNN3 provides a slightly better agreement with 10-m wind speed observations than QNSE and MYNN in the region in both Domains 3 and 4 because it shows slightly lower RMSE and bias values. However, the QNSE simulation represents better the wind speed at 80-m height in Totoral because it shows lower RMSE and bias values. Moreover, QNSE shows a better agreement with temperature observations at all surface weather station locations and at Totoral Wind Farm, as the RMSE, bias, and *R* show.

A more detailed analysis was performed for wind speed forecasts at Totoral Wind Farm because we are interested in predictions at the height of turbines. Density plots between observations and the three WRF simulations show that all simulations overestimate the observed wind speed (Figure 3). However, the QNSE simulation shows less scatter than the other simulations, particularly in the wind speed range 10–16 ms^{-1}, and it

TABLE 3 RMSE and bias for hourly wind speed (WS) and temperature (Temp) forecasts between the three WRF simulations (MYYN, MYNN3, and QNSE) and the weather stations located in Domains 3 (Ch, GM, Ip, QS, and Ra) and 4 (To, Ca, and Ta) for 2013

			MYNN			MYNN3			QNSE		
Station	**Variable**	**magl**	**RMSE**	**Bias**	***R***	**RMSE**	**Bias**	***R***	**RMSE**	**Bias**	***R***
Totoral (To)	WS	80.0	2.6	1.3	0.78	2.6	1.4	0.78	2.4	1.2	0.77
	Temp	77.5	2.5	1.3	0.71	2.5	1.3	0.72	2.3	1.2	0.75
Canela (Ca)	WS	5.0	1.6	0.8	0.73	1.6	0.7	0.71	1.8	0.8	0.74
	Temp	2.0	3.6	2.0	0.78	3.8	2.1	0.77	3.5	1.9	0.79
Talhuen (Ta)	WS	5.0	1.8	0.9	0.08	1.7	0.9	0.08	1.8	1.0	0.08
	Temp	2.0	4.6	3.6	0.56	4.6	3.5	0.55	4.4	3.4	0.57
Chillepin (Ch)	WS	5.0	3.6	1.9	0.79	3.6	1.9	0.78	3.6	1.9	0.81
	Temp	2.0	6.4	−1.2	0.68	6.4	−1.0	0.67	6.3	−1.1	0.70
G. Mistral (GM)	WS	2.0	2.3	1.7	0.77	2.1	1.6	0.76	2.3	1.8	0.80
	Temp	1.5	5.5	4.4	0.78	5.7	4.4	0.77	5.7	4.5	0.80
Illapel (Ip)	WS	2.0	3.3	2.7	0.63	3.3	2.7	0.62	3.4	2.8	0.64
	Temp	1.5	5.9	4.2	0.82	5.9	4.1	0.82	5.7	4.0	0.84
Q. Seca (QS)	WS	2.0	2.7	2.4	0.44	2.6	2.3	0.41	2.7	2.3	0.52
	Temp	1.5	3.8	2.6	0.63	3.8	2.5	0.62	3.6	2.5	0.65
Rapel (Ra)	WS	5.0	2.7	2.0	0.75	2.7	1.9	0.75	3.0	2.2	0.80
	Temp	2.0	5.8	1.7	0.87	5.8	1.7	0.87	5.6	1.6	0.88

Note. The height of the sensors above ground level (agl) is also indicated.
Abbreviations: MYNN, MellorŰYamada Nakanishi and Niino; MYNN3, MYNN Level 3; QNSE, Quasi-Normal Scale Elimination; RMSE, root-mean-square mean; WRF, Weather Research and Forecasting.

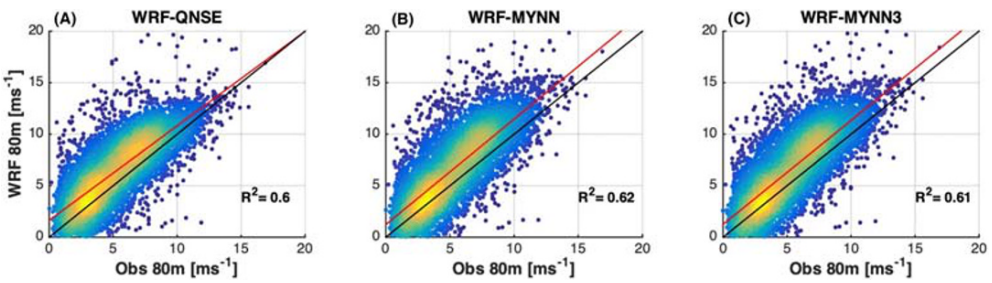

FIGURE 3 Density plots between hourly observations and Weather Research and Forecasting (WRF) simulations using the (A) Quasi-NormalScale Elimination (QNSE), (B) Mellor-Yamada Nakanishi and Niino (MYNN), and (C) MYNN Level 3 (MYNN3) planetary boundary layer (PBL) schemesfor the year 2013. The black and red lines on each panel represent the identity and line arregressi online,respectively. The correlation coefficientis drawn in the lower right of each panel. The yellow and blue colors indicate the higher and lower frequencies of wind speed data, respectively [Colour figure can be viewed at wileyonlinelibrary.com]

shows larger wind speed values closer to observations in the wind speed range 5–10 ms^{-1}. As a result, the calculated regression line (red line) is closer to the 1:1 identity line (black line) for wind speed values larger than 5 ms^{-1} (Figure 3A) compared with MYNN and MYNN3 simulations (Figure 3B,C).

The seasonal evolution of the observed and simulated wind speed at the Totoral Wind Farm during 2013 is assessed in Figure 4. The monthly wind speed from the three simulations shows a similar seasonal evolution as that observed. The monthly RMSE, bias, and *R* values from the three simulations also show a similar behavior among them. The three simulations show the least agreement with observations during winter months (May to August) because the RMSE and bias are larger than 2.5 and 1.3 ms^{-1}, respectively (Figure 4B,C). Besides, the *R* values in all simulations are larger than 0.7 during the year and show their lowest value (<0.7) in June (Figure 4D). The RMSE and bias from the QNSE simulation are lower than the other two simulations for almost the whole year (Figure 4B,C). However, the value of *R* is lower than those shown by the other two simulations in the winter months.

Because rapid hourly and daily wind speed variations are very important for wind power generation, we analyzed how the simulations represent the observed wind speed variations on such small temporal scales. We chose 10 days in January and June because June showed the largest RMSE and bias and the lowest *R* values, whereas January showed, in general, the lowest RMSE and bias and a high *R* value. Thus, we can analyze the performance of the simulations in different atmospheric situations in the year. The observed and simulated wind speed between January 2 and 12, 2013, and between June 15 and 25, 2013, is shown in Figure 5. The observed wind speed in January shows a more regular diurnal pattern than that shown in June, a similar result as that shown by González-Alonso de Linaje[30] in Lengua de Vaca, a coastal site in the Coquimbo region. This may be the result of a weak synoptic forcing in January because the region is dominated by the influence of the South Pacific anticyclone.[4] Because of that, the simulated hourly and daily wind speeds are in closer agreement to observations. On the contrary, the wind speed pattern in June is less stable and cyclic, probably as a result of the influence of higher-latitude perturbations that can reach lower latitudes in winter,

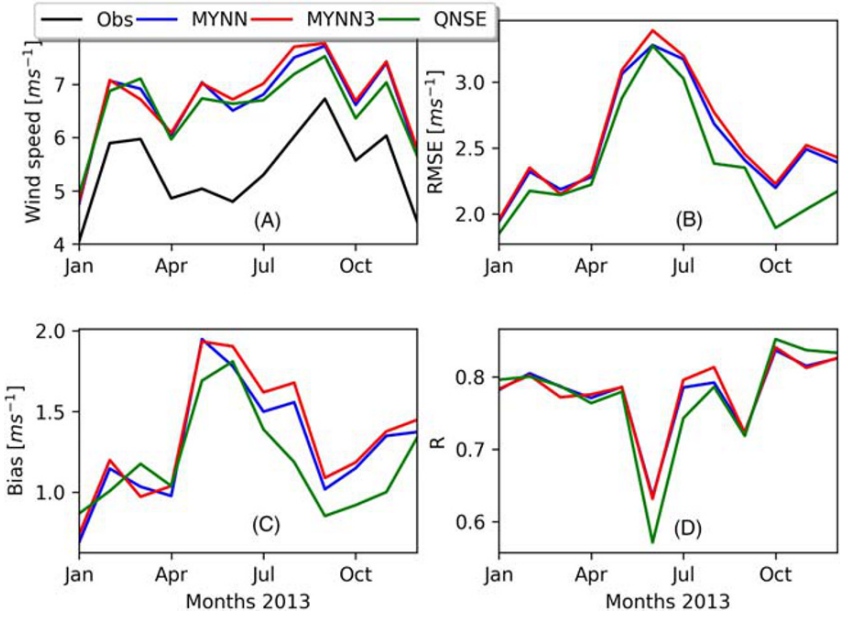

FIGURE 4 Seasonal evolution of (A) wind speeds from observations and the three Weather Research and Forecasting (WRF) simulations, (B) root-mean-square error (RMSE), (C) bias, and (D) *R* between observations and the three WRF forecasts. The comparison was made using hourly data [Colour figure can be viewed at wileyonlinelibrary.com]

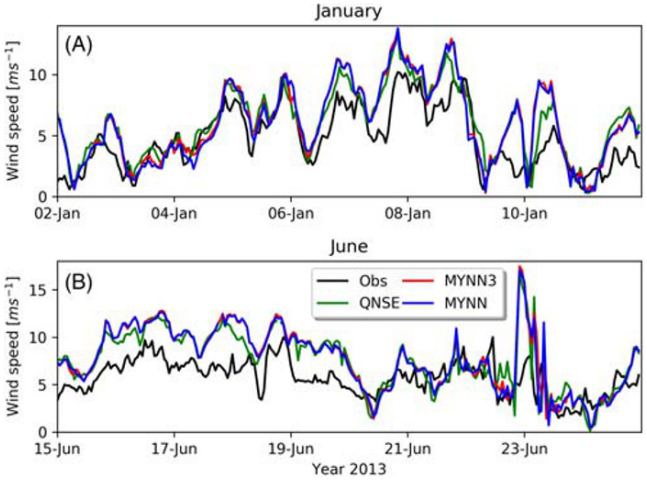

FIGURE 5 Hourly time series of observed and simulated (Quasi-Normal Scale Elimination [QNSE], MellorŰYamada Nakanishi and Niino [MYNN], and MYNN Level 3 [MYNN3]) wind speeds during (A) January 2–12 and (B) June 15–25, 2013, at Totoral Wind Farm [Colour figure can be viewed at wileyonlinelibrary.com]

favored by the northerly displacement of the South Pacific anticyclone, which disrupts the local diurnal cycle observed in January (Figure 5A), causing difficulty in the model to accurately represent it. Despite the three simulations are very close to each other, the QNSE simulation shows a closer agreement to observations than the other simulations on January 3–5, 7–8, and 10, 2013, and also between June 16 and 19, 2013.

The mean wind speed diurnal cycle observed and simulated with the three model configurations averaged over 2013 is shown in Figure 6A. All model configurations follow the same diurnal variation and do not show large differences among them, although they overestimate the wind speed during the whole day. The temporal evolution of RMSE (Figure 6B) and bias (Figure 6C) shows that QNSE and MYNN configurations have the smallest and largest errors, respectively. The bias shows a semidiurnal evolution, with peaks during the early morning and late in the afternoon, probably related to sunrise and sunset times, when the PBL transitions from nocturnal to diurnal and vice versa, which is known to be troublesome for most PBL schemes. The RMSE, bias, and correlation coefficient from the QNSE simulation are 2.4, 1.2, and 0.8, respectively. These values are similar to those found in recent studies in Chile and other regions.[21,22,28,30] It is important to note that QNSE outperforms the other simulations at Totoral mainly during the night and early morning hours maybe indicating its better performance during nighttime hours, as has been suggested by Muñoz et al.,[29] who selected that scheme among others to run WRF model simulations for wind power studies in Chile.

Our results show that MYNN3 is the PBL scheme that better represents the 10-m wind speeds in the region (see RMSE values in Table 3). However, the difference between MYNN3 and QNSE is quite small. On the other hand, QNSE shows a better performance representing the wind speeds at 80-m height in the Totoral Wind Farm, as well as the 2-m temperature over the region except in GM where MYNN shows the lowest RMSE. Therefore, the QNSE scheme was selected to forecast the wind speed at the Totoral Wind Farm and to represent the atmospheric processes in the region. Despite the better agreement of the QNSE configuration with observations at the farm, large errors are present. For that reason, four ANN approaches (d04bp, d03bp, d04pso, and d03pso) were further implemented to test their ability to improve wind speed forecasts and to evaluate the impact of applying the ANN methods to wind speed forecasts from different horizontal resolution simulations. Results from the comparison between raw WRF and ANN-corrected wind speed forecasts with observations during 2014 are shown in the following section.

3.2 | Wind speed forecasts improvement

As described in Section 2.3, four ANN approaches (d04bp, d04pso, d03bp, and d03pso) were implemented to correct raw WRF wind speed forecasts at Totoral. They were evaluated to determine the one that shows the best agreement with observations during the period February to December 2014.

Figure 7A shows the mean diurnal evolution of wind speeds from observations and the four ANN approaches. All ANN approaches show small differences among them with values closer to observations than those shown by raw WRF simulations (Figure 6A). This indicates that any

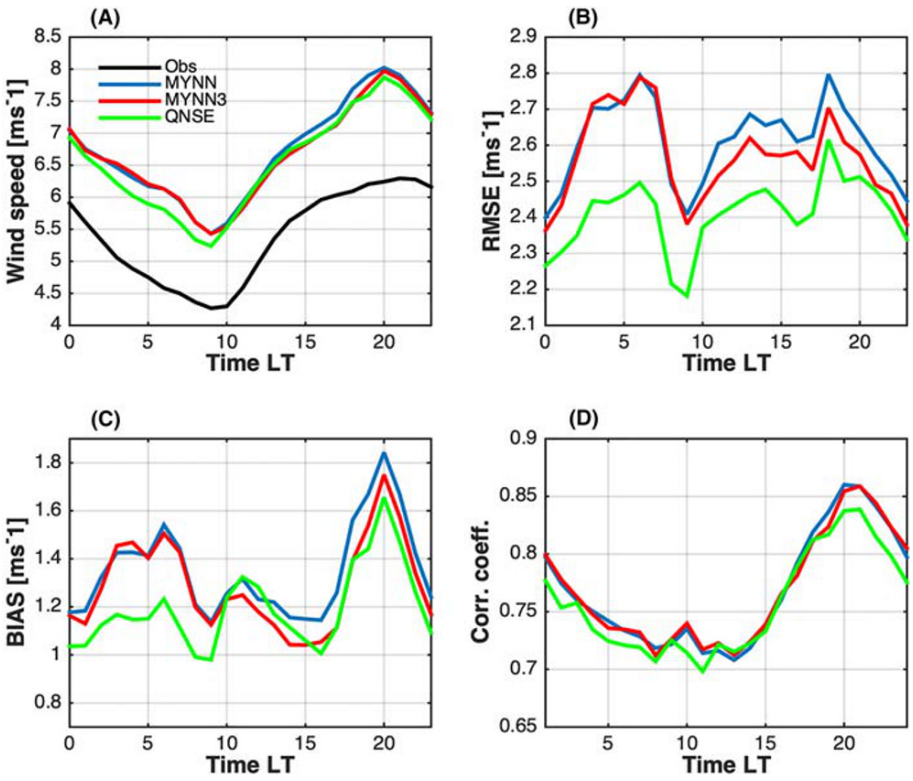

FIGURE 6 Mean diurnal evolution of (A) hourly observed (black line) and simulated wind speeds (color lines), (B) root-mean-square error (RMSE), (C) bias, and (D) *R* between observations and simulations from the three Weather Research and Forecasting (WRF) configurations, averaged over 2013. The blue, red, and green lines correspond to MellorŰYamada Nakanishi and Niino (MYNN), MYNN Level 3 (MYNN3), and Quasi-Normal Scale Elimination (QNSE) simulations, respectively [Colour figure can be viewed at wileyonlinelibrary.com]

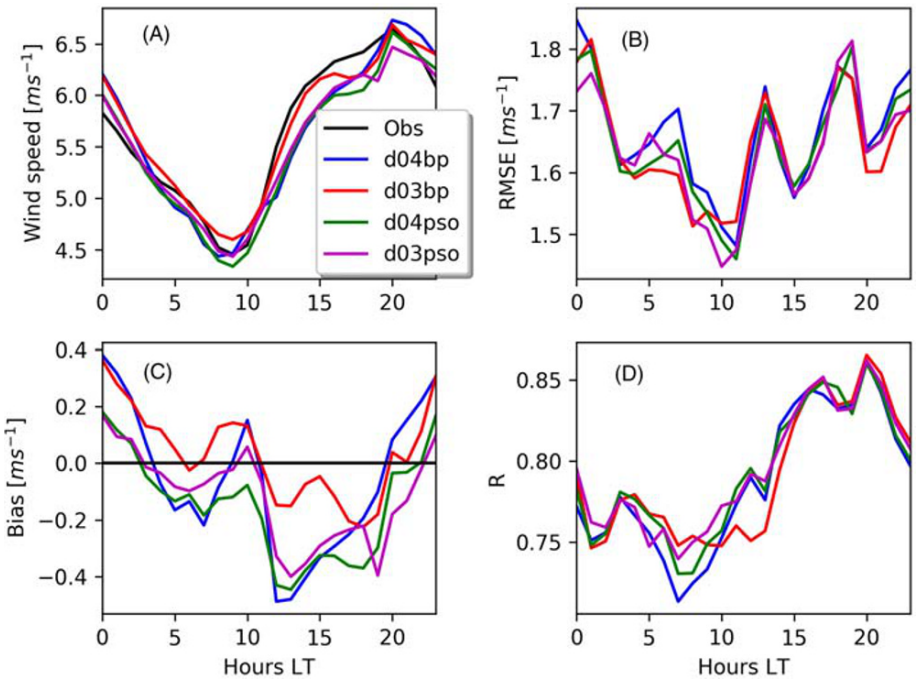

FIGURE 7 Mean diurnal evolution of hourly (A) wind speed from observations and artificial neural network (ANN) approaches and (B) root-mean-square error (RMSE), (C) bias, (D) *R*, between observations and ANN approaches, averaged over the period February to December 2014. See legend for details [Colour figure can be viewed at wileyonlinelibrary.com]

of the ANN approaches could be used as a postprocessing technique, largely reducing the raw WRF forecast errors. In general, the RMSE of all ANN approaches decreases from early morning to 10 LT and increases after that to a maximum at 0LT (Figure 7B). ANN-corrected wind speeds overestimate observations mainly during nighttime, and they underestimate observations during daytime (Figure 7C). In addition, the ANN approaches increase the linear correlations during daytime (Figure 7D).

Table 4 summarizes the results of the comparison between raw WRF forecasts from Domain 3 (d03) and 4 (d04) and the four ANN-corrected forecasts with observations for the test period (February to December 2014). Raw WRF forecasts from Domain 4 (at 1-km horizontal resolution) decreases the RMSE shown by its parent Domain 3 (3-km horizontal resolution), from 2.7 to 2.4 ms^{-1}, indicating the importance of increasing the horizontal resolution in simulations over complex topography. The further postprocessing of wind speed forecasts with any of the four ANN approaches largely decreases the forecast and systematic error (RMSE and bias, respectively) in both domains. However, the different ANN methods only show very small differences between them. The d03bp and d03pso approaches decrease the wind speed forecast errors shown by raw forecasts from Domains 3 and 4 and show a similar performance than d04bp and d04pso. Therefore, using Domain 3 with an ANN method to correct the forecasts has the benefit of using more efficiently the computer resources and providing operational weather forecasts more quickly. On the other hand, the d03pso approach runs faster than d03bp mainly due to its smaller number of neurons in the hidden layer (Table 4). For those reasons, we chose the d03pso approach (ANN fed with the forecasts from Domain 3 and trained with the PSO algorithm) as the postprocessing method to use in the region. From here, afterward, we will use results from d03pso to show the wind speed forecast improvement compared with raw WRF simulations.

As previously mentioned, the performance of wind speed forecasts at the Totoral farm was similar to what has been reported in other studies in Chile and other parts of the world. The RMSE of raw WRF forecasts from Domain d04 is 2.4 ms^{-1} throughout February to December 2014 with a mean overestimation of 1.1 ms^{-1} and an *R* of 0.71. Other studies using high-resolution WRF simulations (between 1- and 5-km horizontal resolutions) have reported an RMSE of 3 ms,[21] 1.9–2.2,[22,28] and 1.75–2.5 ms^{-1},[30] a mean bias of 1.7–2.8 ms^{-1}[21] and an *R* of 0.74[28] and

TABLE 4 RMSE, bias, and correlation coefficient (*R*) between raw wind speed Weather Research and Forecasting (WRF) forecasts from Domain 3 (d03), Domain 4 (d04), forecasts from the four artificial neural network (ANN) approaches (d04bp, d04pso, d03bp, and d03pso), and observations

Parameter	d03	d04	d04bp	d04pso	d03bp	d03pso
RMSE (ms^{-1})	2.68	2.45	1.67	1.65	1.64	1.64
R	0.75	0.76	0.81	0.81	0.81	0.81
Bias (ms^{-1})	1.25	1.12	−0.05	−0.15	0.04	−0.11
Network architecture	-	-	11-5-1	11-14-1	11-17-1	11-8-1

Note. The network architecture (number of neurons per layer) found in each ANN model is also shown. The comparison was made using hourly data.
Abbreviation: RMSE, root-mean-square mean.

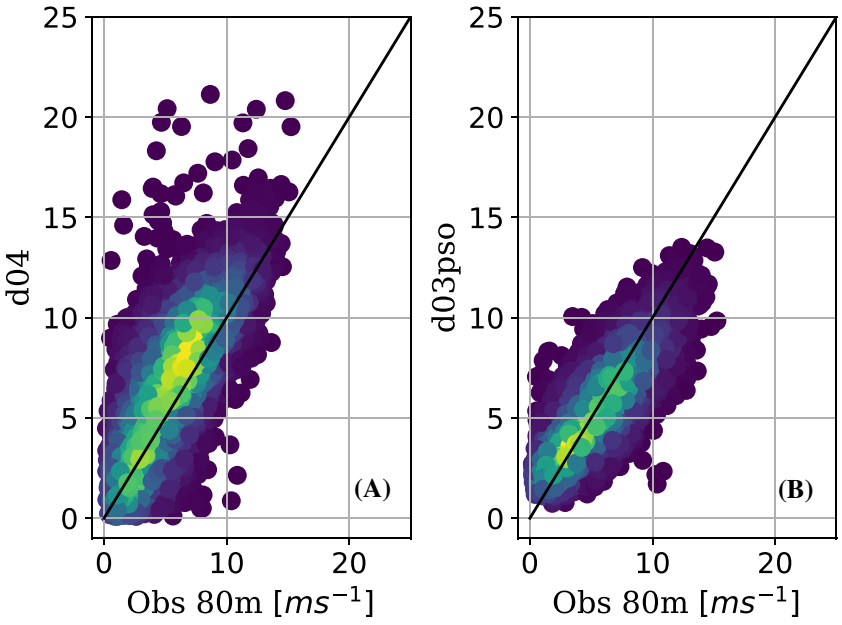

FIGURE 8 Density plots of (A) hourly raw wind speed forecasts (d04) versus hourly observations and (B) hourly artificial neural network(ANN)-corrected wind speed forecasts (d03pso) versus hourly observations at 80-m height in Totoral for the period February to December 2014. The identity line is also drawn. The yellow and blue colors indicate a higher and lower frequencies of wind speed data, respectively [Colour figure can be viewed at wileyonlinelibrary.com]

0.47–0.76.[30] The ANN-corrected wind speed forecasts (d03pso) largely improve the raw forecasts as seen in Figure 8. A much better agreement between d03pso and observations is shown, with a large reduction of the RMSE and bias to 1.6 and −0.1 ms^{-1}, respectively, increasing the value of *R* from 0.76 to 0.81 (Table 4).

Figure 9 shows the seasonal evolution of RMSE, bias, and correlation coefficient between wind speed forecasts (d04 and d03pso) and observations. Moreover, it also shows the skill score between raw and corrected WRF forecasts to analyze the performance of the proposed ANN approach. RMSE values from raw WRF forecasts are larger than 2 ms^{-1} the whole year (except in February), showing the largest values (>3 ms^{-1}) in the austral fall months (April to June 2014) and the smallest values in the austral summer months (Figure 9A). This is likely due to more stable wind speeds in summer months and larger wind speed variability during fall and winter months in the region as a result of the passage of higher latitude cyclonic perturbations.[4] The ANN-corrected forecasts show a large reduction in the RMSE, with values lower than 2 ms^{-1} during the year, even lower than 1.5 ms^{-1} from October to December. The bias from raw WRF forecasts is also largely reduced each month to values close to 0 when the ANN method is applied (9B).

The linear correlation between raw WRF forecasts and observations shows a seasonal evolution during the year with the largest values (>0.75) shown during the austral spring and summer (October to February) and the smallest values (<0.7) shown in the austral fall (Figure 9C), in agreement with the RMSE and bias seasonality. The linear correlation is improved each month by the ANN method, showing values larger than 0.7 during the whole year. The above-mentioned results show that the implementation of the d03pso approach on wind speed forecasts from

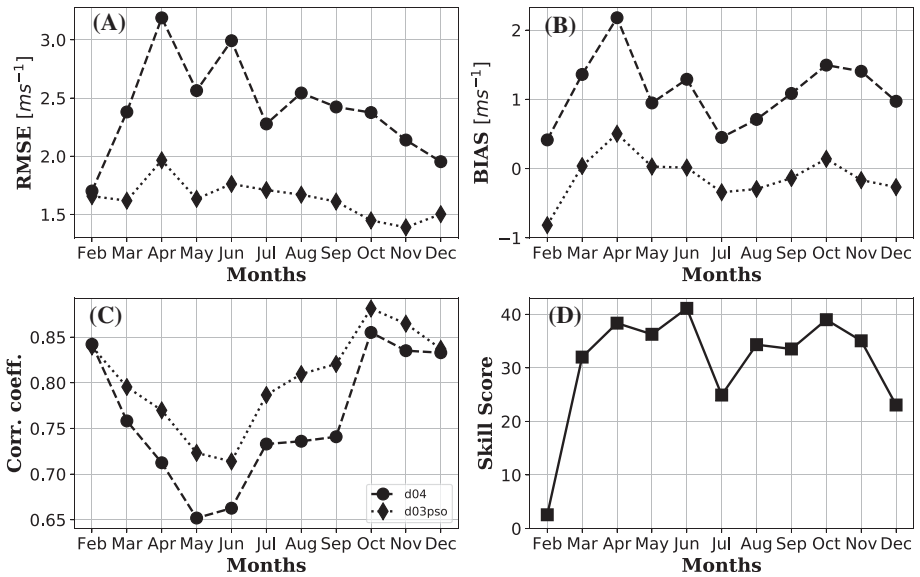

FIGURE 9 Seasonal evolution of (A) root-mean-square error (RMSE), (B) bias, (C) correlation coefficient between raw Weather Research and Forecasting (WRF) (circles) and the artificial neural network (ANN)–corrected (diamonds) forecasts and observations, and (D) the skill score between raw WRF and ANN-corrected forecasts. The comparison was made using hourly data

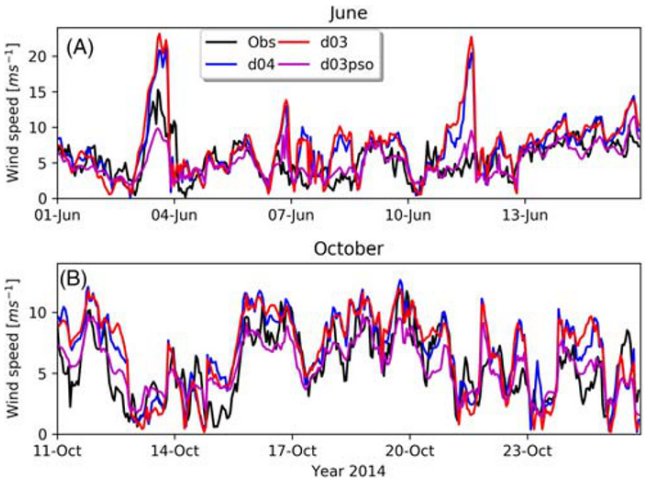

FIGURE 10 Hourly time series of wind speeds from observations, d03, d04, and d03pso during (A) June 1–15 and (B) October 11–25, 2014, at Totoral Wind Farm [Colour figure can be viewed at wileyonlinelibrary.com]

Domain 3 largely improves the raw WRF wind speed forecasts from the higher-resolution Domain 4. This is also indicated by the seasonal evolution of SS (Figure 9D), which ranges between 20% and almost 40% during most of the year.

Time series of wind speeds from observations, from Domains d03 and d04 of raw WRF simulations, and from the d03pso approach were analyzed during 15-day periods of June and October (Figure 10). We chose those months because they showed the largest improvements when the ANN approach was implemented (Figure 9D). Wind speeds in October show a more stable and constant diurnal variation than that shown in June, similar to what was described for January and June 2013 in Figure 5. The d03pso approach better represents the observed wind speed rapid variations most of the time, reducing large errors shown in the raw forecasts, such as those occurring in June 3 and 11 and on October 11–12, 2014.

The cumulative density function (CDF) of absolute errors between observations and forecasts (d04 and d03pso) shows that the number of data with lower errors increases in d03pso compared with raw WRF forecasts (Figure 11). The ANN-corrected forecasts show a much larger number of data where the absolute error was reduced. For example, almost 50% of d03pso forecasts show absolute errors smaller than 1 ms^{-1} compared with less than 40% shown by raw WRF forecasts.

Figure 12 shows the wind speed overestimation in raw WRF forecasts from Domains d03 and d04 during the test period. The model represents well the time of maximum value, although the daily minimum value is simulated 1 h earlier. A much better agreement with observations is obtained by the ANN method (d03pso), not only largely decreasing the overestimation (as previously shown) but also representing better the time when maximum and minimum wind speed values occur during the day.

The RMSE and bias between wind speed observations and forecasts (raw WRF and ANN corrected) were calculated and binned by wind speed observations (Figure 13). The RMSE of raw WRF forecasts decreases in magnitude with increasing wind speed range (Figure 13A). The RMSE from ANN-corrected forecasts is smaller than the RMSE from raw WRF forecasts for wind speeds below 10 ms^{-1}. Notice that this range is where most of the observations are recorded and ANN-corrected forecasts show the best results. For larger wind speed values, raw WRF forecasts show better results. The d03pso approach overestimates observations for wind speeds below 6 ms^{-1}, whereas it underestimates observations for larger wind speed values. For wind speed values larger than 10 ms^{-1}, the forecast underestimation by the d03pso model is very large. The number of wind speed observations above 11 ms^{-1} is not large (6.8% of the data) (Figure 13C), probably limiting the learning

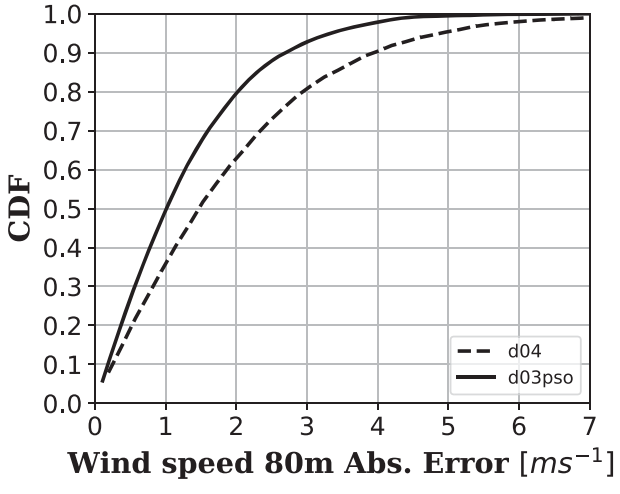

FIGURE 11 Cumulative density function of absolute errors between hourly observations and forecasts (raw Weather Research and Forecasting [WRF] and artificial neural network [ANN] corrected) during February to December 2014

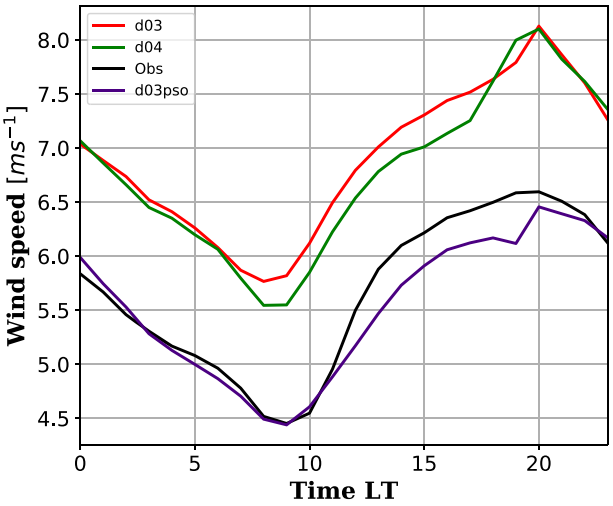

FIGURE 12 Mean diurnal evolution of hourly 80-m wind speed observations, raw Weather Research and Forecasting (WRF) forecasts from Domains 3 and 4, and forecasts corrected by the d03pso method, averaged over the period February to December 2014 [Colour figure can be viewed at wileyonlinelibrary.com]

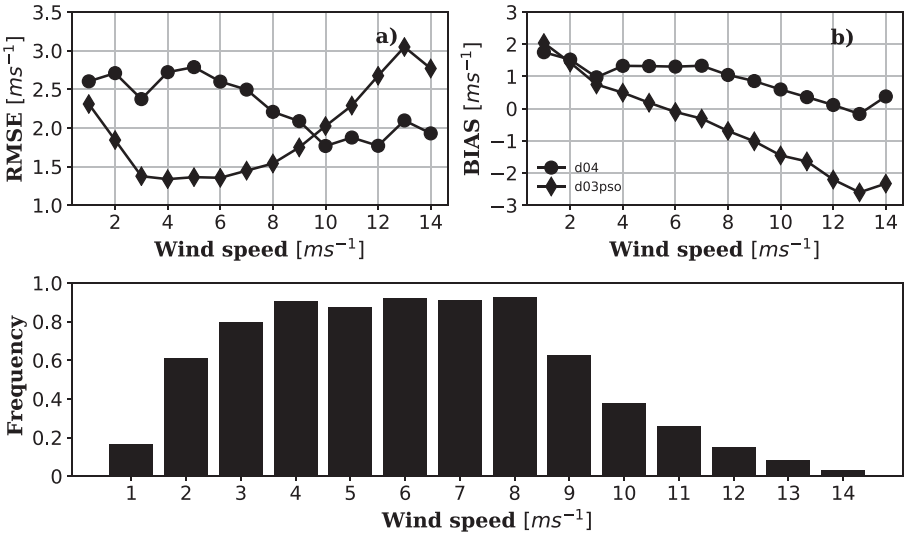

FIGURE 13 (A) Root-mean-square error (RMSE) and (B) bias between hourly wind speed observations and forecasts (raw and artificial neural network [ANN] corrected), and (C) histogram of the number of times with observed hourly wind speeds every 1 ms^{-1}

process of the ANN and, as a consequence, not providing the best estimation for larger wind speed values. However, using a longer training and validation period for the ANN could increase the number of wind speed values over that threshold and improve its performance over that wind speed range.

4 | CONCLUSIONS AND DISCUSSION

The use of wind energy production in Chile has increased over the years. To provide reliable wind power predictions, accurate wind speed forecasts are necessary. To this aim, the mesoscale WRF model was implemented in the region, and its performance was evaluated. Three PBL parameterizations in the WRF model (QNSE, MYNN, and MYNN3) were compared with observations for 1 year (2013) to determine the one that best represents the wind field at the Totoral wind farm.

Wind speed forecasts from the WRF model show similar performance at Totoral Wind Farm as those reported in other studies in Chile and other parts of the world.[28,30,60] Several factors have been documented to affect the performance of wind speed forecasts from numerical models over complex topography: the misrepresentation of the real topography in the model, the incomplete understanding of the physical processes that challenge the accurate representation of the local atmospheric circulations, and the scarce observations, in a lesser extent.[18,19,60,61]

As a result of model evaluation, we chose the QNSE scheme due to its better agreement with observations at the Totoral farm, showing a bias lower than 1.2 ms^{-1} and an RMSE of 2.4 ms^{-1}. Because large errors in numerical forecasts are still present, having a method to reduce them is desirable. We tested two ANN models based on BP and PSO methods, which were applied to Domains 3 and 4 of the WRF configuration chosen (QNSE), representing four postprocessing approaches to be evaluated. Raw wind speed forecasts from Domain 4 show a better performance than

raw forecasts from Domain 3, as Table 3 indicates. The wind speed RMSE and bias errors are lower than 2.5 and 1.3 ms^{-1}, respectively, in Domain 4, while there are lower than 3.6 and 3 ms^{-1}, respectively, in Domain 3. The reduction of 1 ms^{-1} in the RMSE using a 1 × 1-km horizontal resolution domain highlights the importance of using higher-resolution simulations to forecast near-surface circulations over complex terrain. The four ANN approaches largely decreased the raw forecast errors in Domains 3 and 4. For example, both ANN methods applied to Domain 3 (coarser resolution) showed a much better performance than raw forecasts from Domain 4 (higher horizontal resolution). Furthermore, the two ANN approaches that corrected forecasts from the coarser horizontal resolution domain (d03) showed similar performances as the two ANN approaches that corrected forecasts from the higher-resolution domain (d04). These results indicate that instead of using a WRF configuration with four domains, providing higher-resolution forecasts for the region, we can use a WRF configuration with only three domains and apply one of the ANN methods to Domain 3 as a postprocessing technique to reduce the errors. Among the two ANN methods applied to Domain 3, we chose the PSO method because it can be calculated with much less computational effort because it uses a lower number of neurons in the hidden layer. Wind speed forecasts from the WRF model using three nested domains and an ANN to postprocess its output reduce the simulation time in more than 75% compared with a WRF configuration with four domains, saving, therefore, computational resources, and being able to provide wind speed forecasts in advance.

Results from this study show that an ANN optimized with the PSO algorithm may be used as a reliable tool to obtain wind speed forecasts in the Coquimbo region, where most of the wind energy production in Chile is installed. Mattar and Borvarán[28] obtained an RMSE value of 2.2 ms^{-1} from WRF simulations at 3-km horizontal resolutions in a coastal location further south. González-Alonso de Linaje et al.[30] obtained RMSE values between 1.75 and 2.5 ms^{-1} for 2 months in a coastal site in the Coquimbo region. We obtained an RMSE value of 2.4 ms^{-1} at Totoral Wind Farm in this study, using high-resolution (1-km) simulations during a year of evaluation. However, the RMSE was largely decreased to 1.6 ms^{-1} when the ANN method is applied to coarser-resolution forecasts, representing an RMSE reduction of 20–40% for almost the whole year. This highlights the good performance of the model in the region and the large improvement that can be achieved using this method, which can help to provide accurate and reliable wind energy forecasts in the future.

It is important to note that the ANN methods used in this study were applied to a single point in a wind farm, largely reducing the raw forecast errors. We believe that applying one of the ANN methods employed in this study to wind speed forecasts at any other location in the region should reduce the forecast errors and improve the wind speed regional representation. However, this needs to be evaluated using all the observations available in the region to quantify the degree of forecast improvement and its relation with topographic characteristics.

ACKNOWLEDGEMENTS

This work was supported by the FONDEF IDeA ID14I10016 project. We thank Latin American Power (LAP) for useful information. I. Salfate acknowledges Dirección de Investigación y Desarrollo de la Universidad de La Serena University (DIDULS) through the research project PI15141 and the Departamento de Física y Astronomía of Universidad de La Serena for supporting this research. J.C. Marín and O. Cuevas thank the Centro de Estudios Atmosféricos y Astroestadística (CEAAS) of Universidad de Valparaíso for supporting this research.

CONFLICT OF INTERESTS

The authors declare that there are no conflict of interests regarding the publication of this paper.

ORCID

Ignacio Salfate https://orcid.org/0000-0001-8125-7294
Julio C. Marin https://orcid.org/0000-0001-8112-722X

REFERENCES

1. Amjady N, Keynia F, Zareipour H. Short-term wind power forecasting using ridgelet neural network. *Electr Power Syst Res*. 2011;81(12):2099-2107.
2. Manwell JF, McGowan JG, Rogers AL. *Wind Energy Explained: Theory, Design and Application*. Hoboken, NJ: John Wiley & Sons; 2010:704.
3. Montecinos S, Gutiérrez J, López-Cortés F, López D. Climatic characteristics of the semi-arid Coquimbo region in Chile. *J Arid Environ*. 2016;126:7-11.
4. Rahn D, Garreaud R. A synoptic climatology of the near-surface wind along the west coast of South America. *Int J Climatology*. 2013;34:3628-3647.
5. Barrett BS, Hameed S. Seasonal variability in precipitation in central and southern Chile: modulation by the South Pacific high. *J Climate*. 2017;30(1):55-69.
6. Rutllant J, Fuenzalida H. Synoptic aspects of the central Chile rainfall variability associated with the Southern Oscillation. *Int J Climatology*. 1991;11(1):63-76.
7. Montecinos A, Aceituno P. Seasonality of the ENSO-related rainfall variability in central Chile and associated circulation anomalies. *J Climate*. 2003;16(2):281-296.
8. Juliá C, Rahn DA, Rutllant JA. Assessing the influence of the MJO on strong precipitation events in subtropical, semi-arid north-central Chile (30° S). *J Climate*. 2012;25:7003-7013.
9. Barrett BS, Carrasco JF, Testino AP. Madden–Julian oscillation (MJO) modulation of atmospheric circulation and Chilean winter precipitation. *J Climate*. 2012;25(5):1678-1688.

10. Rahn D. Influence of large scale oscillations on upwelling-favorable coastal wind off central Chile. *J Geophys Res*. 2012;117:D19114.
11. Kalthoff N, Bischoff-gauß I, Fiebig-Wittmaack M, et al. Mesoscale wind regimes in Chile at 30 S. *J Appl Meteorology*. 2002;41(9):953-970.
12. Costa A, Crespo A, Navarro J, Lizcano G, Madsen H, Feitosa E. A review on the young history of the wind power short-term prediction. *Renew Sustain Energy Rev*. 2008;12(6):1725-1744.
13. Lei M, Shiyan L, Chuanwen J, Hongling L, Yan Z. A review on the forecasting of wind speed and generated power. *Renew Sustain Energy Rev*. 2009;13(4):915-920.
14. Aggarwal S, Gupta M. Wind power forecasting: a review of statistical models–wind power forecasting. *Int J Energy Sci*. 2013;3(1):1-10.
15. Chang WY. A literature review of wind forecasting methods. *J Power Energy Eng*. 2014;2(4):161–168.
16. Storm B, Dudhia J, Basu S, Swift A, Giammanco I. Evaluation of the weather research and forecasting model on forecasting low-level jets: implications for wind energy. *Wind Energy: An Int J Progress Appl Wind Power Conv Technol*. 2009;12(1):81-90.
17. Storm B, Basu S. The WRF model forecast-derived low-level wind shear climatology over the United States Great Plains. *Energies*. 2010;3(2):258-276.
18. Jiménez PA, Dudhia J. Improving the representation of resolved and unresolved topographic effects on surface wind in the WRF model. *J Appl Meteor Climatol*. 2012;51:300-316.
19. Jiménez PA, Dudhia J, González-Rouco JF, et al. An evaluation of WRF's ability to reproduce the surface wind over complex terrain based on typical circulation patterns. *J of Geophys Res*. 2013;118:7651-7669.
20. Marín JC, Pozo D, Mlawer E, Turner D, Curé M. Dynamics of local circulations in mountainous terrain during the RHUBC-II project. *Monthly Weather Rev*. 2013;141:3641-3656.
21. Carvalho D, Rocha A, Gómez-Gesteira M, Santos C. A sensitivity study of the WRF model in wind simulation for an area of high wind energy. *Environ Modell Softw*. 2012;33:23-34.
22. Carvalho D, Rocha A, Gómez-Gesteira M, Santos CS. Sensitivity of the WRF model wind simulation and wind energy production estimates to planetary boundary layer parameterizations for onshore and offshore areas in the Iberian Peninsula. *Appl Energy*. 2014;135:234-246.
23. Draxl C, Hahmann A, Peña A, Giebel G. Evaluating winds and vertical wind shear from Weather Research and Forecasting model forecasts using seven planetary boundary layer schemes. *Wind Energy*. 2014;17:39-55.
24. Penchah MM, Malakooti H, Satkin M. Evaluation of planetary boundary layer simulations for wind resource study in east of Iran. *Renew Energy*. 2017;111:1-10.
25. Watts D, Jara D. Statistical analysis of wind energy in Chile. *Renew Energy*. 2011;36(5):1603-1613.
26. Morales L, Lang F, Mattar C. Mesoscale wind speed simulation using CALMET model and reanalysis information: an application to wind potential. *Renew Energy*. 2012;48:57-71.
27. Watts D, Durán P, Flores Y. How does El Niño Southern Oscillation impact the wind resource in Chile? A techno-economical assessment of the influence of El Niño and La Niña on the wind power. *Renew Energy*. 2017;103:128-142.
28. Mattar C, Borvarán D. Offshore wind power simulation by using WRF in the central coast of Chile. *Renew Energy*. 2016;94:22-31.
29. Muñoz RC, Falvey MJ, Arancibia M, et al. Wind energy exploration over the Atacama Desert: a numerical model-guided observational program. *Bull Am Meteorological Soc*. 2018;99(10):2079-2092.
30. González-Alonso de Linaje N, Mattar C, Borvarán D. Quantifying the wind energy potential differences using different WRF initial conditions on Mediterranean coast of Chile. *Energy*. 2019;188:116017.
31. Muñoz RC, Falvey MJ, Araya M, Jacques-Coper M. Strong down-valley low-level jets over the Atacama Desert: observational characterization. *J Appl Meteorology Climatology*. 2013;52(12):2735-2752.
32. Sailor D, Hu T, Li X, Rosen J. A neural network approach to local downscaling of GCM output for assessing wind power implications of climate change. *Renew Energy*. 2000;19(3):359-378.
33. Lima FJ, Martins FR, Pereira EB, Lorenz E, Heinemann D. Forecast for surface solar irradiance at the Brazilian northeastern region using NWP model and artificial neural networks. *Renew Energy*. 2016;87:807-818.
34. Lauret P, Diagne HM, David M. A neural network post-processing approach to improving NWP solar radiation forecasts. *Energy Procedia*. 2014;57:1044-1052.
35. Barbounis TG, Theocharis JB, Alexiadis MC, Dokopoulos PS. Long-term wind speed and power forecasting using local recurrent neural network models. *IEEE Trans Energy Conv*. 2006;21(1):273-284.
36. Kusiak A, Zheng H, Song Z. Wind farm power prediction: a data-mining approach. *Wind Energy: An Int J Progress Appl Wind Power Conv Technol*. 2009;12(3):275-293.
37. Catalão JPdS, Pousinho HMI, Mendes VMF. Short-term wind power forecasting in Portugal by neural networks and wavelet transform. *Renew Energy*. 2011;36(4):1245-1251.
38. Kennedy J, Eberhart R. Particle swarm optimisation. In: Proceedings of the IEEE International Conference of Neural Network (ICNN'95), Vol. IV; 1995; Perth, WA:1942-1948.
39. Pookpunt S, Ongsakul W. Optimal placement of wind turbines within wind farm using binary particle swarm optimization with time-varying acceleration coefficients. *Renew Energy*. 2013;55:266-276.
40. Kongnam C, Nuchprayoon S. A particle swarm optimization for wind energy control problem. *Renew Energy*. 2010;35(11):2431-2438.
41. Liao CC, Zhao XL, Xu JZ. Blade layers optimization of wind turbines using FAST and improved PSO algorithm. *Renew Energy*. 2011;42:227-233.
42. Liu Feng-Jiao, Chen Pai-Hsun, Kuo Shyi-Shiun, De-Chuan Su, Chang Tian-Pau, Yu-Hua Yu, Algorithm Tsung-ChiLin.. Wind characterization analysis incorporating genetic a case study in Taiwan Strait. *Energy*. 2011;36(5):2611-2619.
43. Nunalee CG, Basu S. Mesoscale modeling of coastal low-level jets: implications for offshore wind resource estimation. *Wind Energy*. 2014;17(8):1199-1216.
44. Louka P, Galanis G, Siebert N, et al. Improvements in wind speed forecasts for wind power prediction purposes using Kalman filtering. *J Wind Eng Indust Aerodyn*. 2008;96(12):2348-2362.
45. Skamarock WC, Klemp JB, Dudhia J, et al. A description of the Advanced Research WRF Version 3. tech. rep., University Corporation for Atmospheric Research, Boulder Colorado. NCAR Tech. Note; 2008.
46. Nakanishi M, Niino H. An improved Mellor–Yamada level 3 model: its numerical stability and application to a regional prediction of advecting fog. *Bound-Layer Meteorol*. 2006;119:397-407.

47. Nakanishi M, Niino H. Development of an improved turbulence closure model for the atmospheric boundary layer. *J Meteorol Soc Japan Ser II*. 2009;87:895-912.
48. Sukoriansky S, Galperin B, Perov V. Application of a new spectral theory of stably stratified turbulence to atmospheric boundary layers over sea ice. *Bound-Layer Meteorol*. 2005;117:231-257.
49. Mlawer EJ, Taubman SJ, Brown PD, Iacono MJ, Clough SA. Radiative transfer for inhomogeneous atmospheres: RRTM, a validated correlated-k model for the longwave. *J Geophys Res: Atmos*. 1997;102(D14):16663-16682.
50. Dudhia J. Numerical study of convection observed during the winter monsoon experiment using a mesoscale two-dimensional model. *J Atmos Sci*. 1989;46(20):3077-3107.
51. Chen F, Dudhia J. Coupling an advanced land surface-hydrology model with the Penn State-NCAR MM5 modeling system part I: model implementation and sensitivity. *Monthly Weather Rev*. 2001;129(4):569-585.
52. Hong S, Dudhia J, Chen SH. A revised approach to ice-microphysical processes for the bulk parameterization of cloud and precipitation. *Monthly Weather Rev*. 2004;132:103-120.
53. Kain JS. The Kain–Fritsch convective parameterization: an update. *J Appl Meteorol*. 2004;43:170-181.
54. Lazzús JA. ρ–T–P prediction for ionic liquids using neural networks. *J Taiwan Inst Chem Eng*. 2009;40(2):213-232.
55. Hagan MT, Menhaj MB. Training feedforward networks with the Marquardt algorithm. *IEEE Trans Neural Netw*. 1994;5(6):989-993.
56. Zupan J, Gasteiger J. *Neural Networks for Chemists: An Introduction*. Hoboken, NJ: John Wiley & Sons Inc; 1993:305.
57. Eberhart R, Kennedy J. Particle swarm optimization. *Proc IEEE Int Conf Neural Netw*. 1995;4:1942-1948.
58. Lazzús JA, Salfate I, Montecinos S. Hybrid neural network–particle swarm algorithm to describe chaotic time series. *Neural Netw World*. 2014;24(6):601.
59. Wilks DS. *Statistical methods in the atmospheric sciences*. Vol. 100, 3rd ed. Cambridge, MA: Academic Press; 2011:704.
60. Siuta D, West G, Stull RWRF. Hub-height wind forecast sensitivity to PBL scheme, grid length, and initial condition choice in complex terrain. *Bull Am Meteorol Soc*. 2017;32:493-509.
61. Chow FK, Snyder BJ, De Wekker SFJ. *Mountain Weather Research and Forecasting: Recent Progress and Current Challenges*. New York: Springer; 2013:750.

How to cite this article: Salfate I, Marin JC, Cuevas O, Montecinos S. Improving wind speed forecasts from the Weather Research and Forecasting model at a wind farm in the semiarid Coquimbo region in central Chile. *Wind Energy*. 2020;1–16. https://doi.org/10.1002/we.2527